Interlayer coupling in the superconducting state of iron-based superconductors

Wenshan Hong,[1,2,3,*] Honglin Zhou,[1,2,*] Zezhong Li,[1,2] Yang Li,[1,2] Uwe Stuhr,[4] Amit Pokhriyal,[5,6] Haranath Ghosh,[5,6,†] Zhen Tao,[7] Xingye Lu,[7] Jiangping Hu,[1,2,8] Shiliang Li,[1,2,8,‡] and Huiqian Luo[1,8,§]

[1]*Beijing National Laboratory for Condensed Matter Physics, Institute of Physics, Chinese Academy of Sciences, Beijing 100190, China*
[2]*University of Chinese Academy of Sciences, Beijing 100049, China*
[3]*International Center for Quantum Materials, School of Physics, Peking University, Beijing 100871, China*
[4]*Laboratory for Neutron Scattering and Imaging, Paul Scherrer Institut, CH-5232 Villigen PSI, Switzerland*
[5]*Human Resources Development Section, Raja Ramanna Centre for Advanced Technology, Indore 452013, India*
[6]*Homi Bhabha National Institute, BARC training school complex 2nd floor, Anushakti Nagar, Mumbai 400094, India*
[7]*Center for Advanced Quantum Studies and Department of Physics, Beijing Normal University, Beijing 100875, China*
[8]*Songshan Lake Materials Laboratory, Dongguan, Guangdong 523808, China*

(Received 12 August 2022; revised 8 June 2023; accepted 12 June 2023; published 21 June 2023)

High-temperature superconducting paring is generally believed to be mediated by the magnetic fluctuations that mostly occur within the two-dimensional conducting layers (Cu-O, Fe-As, or Fe-Se) in copper oxides, iron pnictides, iron chalcogenides, etc. Here, on the basis of inelastic neutron scattering measurements on a superconducting iron pnictide $Ca_{0.33}Na_{0.67}Fe_2As_2$, we have discovered a highly three-dimensional spin resonance mode with upward V-shape dispersions both in the *ab* plane and along the *c* axis. The superconducting gaps exhibit strong k_z modulations involved with significant changes on the size of one hole pocket and the density state of the d_{z^2} orbital of Fe. The resonance dispersions don't always seem confined by the total gaps summed on those imperfectly nesting Fermi sheets. It is demonstrated that the *c*-axis dependence of both the resonance energy and its intensity in iron pnictides can be universally scaled with the distance between two adjacent Fe-As layers (d), and the k_z modulation of the gap is also anticorrelated with d. These results highlight the role of interlayer coupling in iron-based superconductivity, suggesting that the interlayer pairing may also be driven by magnetic fluctuations under certain spin-orbit couplings.

DOI: 10.1103/PhysRevB.107.224514

I. INTRODUCTION

Currently, there are only two families of unconventional superconductors that could show high-T_c superconductivity above 40 K under ambient pressure, i.e., cuprates and iron-based superconductors (FeSCs) [1–7]. Both of them have quasi-two-dimensional (quasi-2D) layered structures (Cu-O, Fe-As, or Fe-Se layers) with strong antiferromagnetic (AFM) fluctuations; thus, it is speculated that they may share a common superconducting pairing mechanism [8–11]. Indeed, this is well supported by an extensively observed spin resonance mode (SRM) in the neutron-scattering results of both families, which is defined by a sharp peak in the magnetic excitations around the AFM ordering wave vector in the superconducting state with an order-parameter-like intensity [12–41]. The mode energy of the resonance (namely, resonance energy E_R) linearly scales with T_c having similar ratios for FeSCs ($E_R/k_BT_c = 4.9$) and cuprates ($E_R/k_BT_c = 5.8$), where k_B is the Boltzmann factor [29–33].

Theoretically, the SRM is usually interpreted as a singlet-to-triplet exciton from the quasiparticle excitations between the sign-reversed gapped Fermi surfaces [42–47]. In this picture, the distribution of the resonance intensity should be mostly beneath the total superconducting gaps summed on these two parts of Fermi sheets: $\Delta_{\rm tot} = |\Delta_{\mathbf{k}}| + |\Delta_{\mathbf{k+Q}}|$ [32,34,48,49], where $\mathbf{k}$ is the electron momentum in the reciprocal space and $\mathbf{Q}$ is the momentum transfer in between two Fermi sheets. The dispersions of SRM in the energy-momentum space highly depend on the pairing characters associated with the dynamic AFM correlations in the superconducting state [37–40]. Specifically, in the case of single-band cuprates, the SRM shows a downward dispersion determined by the domelike distribution of the d-wave gap [here $\Delta_{\rm tot} = 2|\Delta| = \Delta_0|\cos(k_x) - \cos(k_y)|$]. The whole magnetic excitations form an hour-glass shape together with the upward dispersion of the spin waves in the normal state, where the neck is hosted by the resonance peak at E_R [14,42]. In the multiband FeSCs with isotropic $s^{\pm}$-wave pairing symmetry, the total gap summed on one pair of hole-electron Fermi pockets ($\Delta_{\rm tot} = |\Delta_n| + |\Delta_p|$) forms a $\mathbf{Q}$-independent "flat ceiling" instead, where the two gaps are quasi-2D and may have different magnitudes [32]. Thus, the SRM with peak energy $E_R < \Delta_{\rm tot}$ is predicted to show a magnonlike upward in-plane dispersion, which should be determined by the normal state spin velocities and further influenced by the anisotropic Landau dampings in the superconducting state [37–40].

Although the superconducting pairing mostly occurs within the Cu–O layers in cuprates, the interlayer coupling is also argued to boost T_c by promoting the superfluid density and stabilizing the phase coherence of Cooper pairs [1,7,50].

*These authors contributed equally to this work.
†hng@rrcat.gov.in
‡slli@iphy.ac.cn
§hqluo@iphy.ac.cn

Indeed, the optimal T_c is significantly enhanced from the single layer, bilayer to trilayer systems in those Bi-, Tl- and Hg-based compounds [51–55]. However, a similar pattern in FeSCs no longer exists [3,56,57]. For example, the bilayer systems such as 122-type, 1144-type, and 12442-type iron pnictides do not have higher T_c than those single-layered 1111-type compounds [56–61], and the maximum T_c ($\sim$55 K) of bulk FeSCs seems far below the record of cuprates ($\sim$134 K) under ambient pressure [54,58]. In fact, comparing to the quasi-2D nature of cuprates, the FeSCs are more complicated due to their nearly three-dimensional (3D) superconductivity and magnetism [9,62]. Their multiband Fermi surfaces are contributed differently by the density of states (DOS) by all five orbitals of Fe^{2+} [63–68]. Their superconducting gaps $\Delta_{\mathbf{k}}$ not only show strong **k**-dependencies within the $[k_x, k_y]$ plane among different Fermi pockets but also disperse along k_z together with the modulations of their pocket sizes [69,70]. This means that $\Delta_{\rm tot}$ actually has multiple **Q** distributions smeared by its k_z modulation, instead of the flat **Q**-independent distribution in the quasi-2D cases [63]. However, the SRM seems randomly to show a c-axis dispersion in FeSCs [21–41], and its in-plane dispersion exhibits either an upward- or downwardlike shape probably irrelevant to the gap distributions [32,37,40]. Such cases make it a great challenge to describe the magnetically driven paring process both in cuprates and FeSCs under a unified picture.

Here, in this paper, on the basis of measurements on a 3D SRM in $Ca_{0.33}Na_{0.67}Fe_2As_2$ and comparison with other compounds, we demonstrate that the interlayer coupling is a key to unknot the above puzzles in FeSCs, where both the c-axis dispersion of SRM and the gap modulations can be universally scaled with the distance between the nearest Fe-As layers (d). The SRM exhibits a quasi-2D character when d is larger than 6.7 Å, its in-plane dispersion is mainly determined by the nesting wave vectors with different gaps and pocket sizes under a weak-coupling approach. On the contrary, the SRM exhibits a 3D character for small d cases, both in-plane and c-axis dispersions basically follow the V-shape of the spin waves in the normal state under a strong-coupling approach, while the spin velocities are different from the normal state and the resonance intensity may not always be confined by the gap distributions. We argue that both the inter- and intralayer pairings may be driven by magnetic fluctuations but involved with different orbital contributions in iron-pnictide superconductors, the competition in between them related to the Fe-As layer distance significantly affects superconductivity apart from the charge doping effects. These results provide a phenomenological understanding on the relationship between the local crystalline structure and the multiband high-T_c superconductivity in layered FeSCs. It means that their superconductivity is more tunable than the doped Mott insulator case in cuprates, but their maximum T_c is limited by the presence of interlayer coupling.

II. EXPERIMENTS AND METHODS

A. Crystal growth and characterization

The $Ca_{1-x}Na_xFe_2As_2$ system is a 122-type FeSC with a short Fe-As layer distance ($d = 5.995$ Å) due to the small radius of Ca [inset of Fig. 1(a)]. It has a stripe-type antiferromagnetism in the parent compound, a C_4 phase magnetism in the underdoped region, and an optimal $T_c \approx 35$ K around $x = 0.67$ [Fig. 1(a)] [71]. The $Ca_{0.33}Na_{0.67}Fe_2As_2$ single crystals were grown with the NaAs-flux method according to previous reports [71–74]; the details of the procedure and characterization were published in Ref. [74]. Three precursors NaAs, CaAs, and Fe_2As were first prepared with highly pure raw materials Na($>99.5\%$), Ca($>99.9\%$), Fe($>99.5\%$), and As($>99.99\%$) by solid-state reaction method, then they were mixed together at a molar ratio of CaAs : Fe_2As : NaAs $= 0.33 : 1 : 3.67$ to grow single crystals in a box furnace. The typical sizes of the crystals were about $5 \sim 15$ mm in the ab plane and 0.5 mm for thickness along the c axis. The orientation of each crystal used in this study was carefully checked by using an x-ray Laue camera. Figure 1(b) shows the zero-field-cooling magnetization in six randomly selected samples; all of them have full diamagnetism at low temperature and sharp superconducting transitions with an average $T_c = 34.2 \pm 0.5$ K. There are no anomalies in the resistivity measurements above T_c [74], suggesting the absence of structural or magnetic phase transition that exists in the parent compound $CaFe_2As_2$.

B. Neutron scattering experiments

Neutron scattering experiments were carried out using thermal triple-axis spectrometer EIGER at the Swiss Spallation Neutron Source, Paul Scherrer Institut, Switzerland [75]. We defined the wave vector **Q** at (q_x, q_y, q_z) as $(H, K, L) = (q_x a/2\pi, q_y b/2\pi, q_z c/2\pi)$ reciprocal lattice units using the same magnetic unit cell as the parent compound [3]: $a = b = 5.44$ Å, $c = 11.99$ Å. The scattering plane was set up as $[H, 0, 0] \times [0, 0, L]$, where the AFM wave vector locates at $\mathbf{Q}_{\rm AFM} = [1, 0, L]$ ($L = \pm1, \pm3, \pm5$). We coaligned about 5.8 grams of single crystals on several aluminum plates [inset of Fig. 1(b)]. Before the inelastic measurements, elastic neutron scattering was used to assess the quality and mosaic of the crystal array. The zero flat signal in Fig. 1(c) shown by the difference between $T = 1.5$ K and $T = 40$ K at $Q = (1, 0, 1)$ and $Q = (1, 0, 3)$ indicates the absence of stripe-type AFM order. The total mosaic was determined by the full width at half maximum (FWHM) of rocking curves at $(2, 0, 0)$ and $(0, 0, 4)$, which is about 3.3° in the ab plane and 3.1° for out-of-plane case, respectively [inset of Fig. 1(c)]. Such a sample mosaic is sufficient to satisfy the criteria of inelastic neutron scattering (INS) experiments. The data were collected with a final energy fixed as $E_f = 14.8$ meV in energy loss measurement mode ($E_i > E_f$), with a 37-mm-thick pyrolytic graphite filter, a double focusing monochromator, and a horizontal focusing analyzer.

C. Density-functional-theory calculations

To figure out the k_z modulations of the orbital characters in $Ca_{0.33}Na_{0.67}Fe_2As_2$, we performed density functional theory (DFT) calculations with a plane-wave basis set. Single point energy calculations are performed using the experimental lattice parameters as input. Based on the QUANTUM ESPRESSO code, we employed ultrasoft pseudopotential and self-consistent field approaches in our calculations [76].

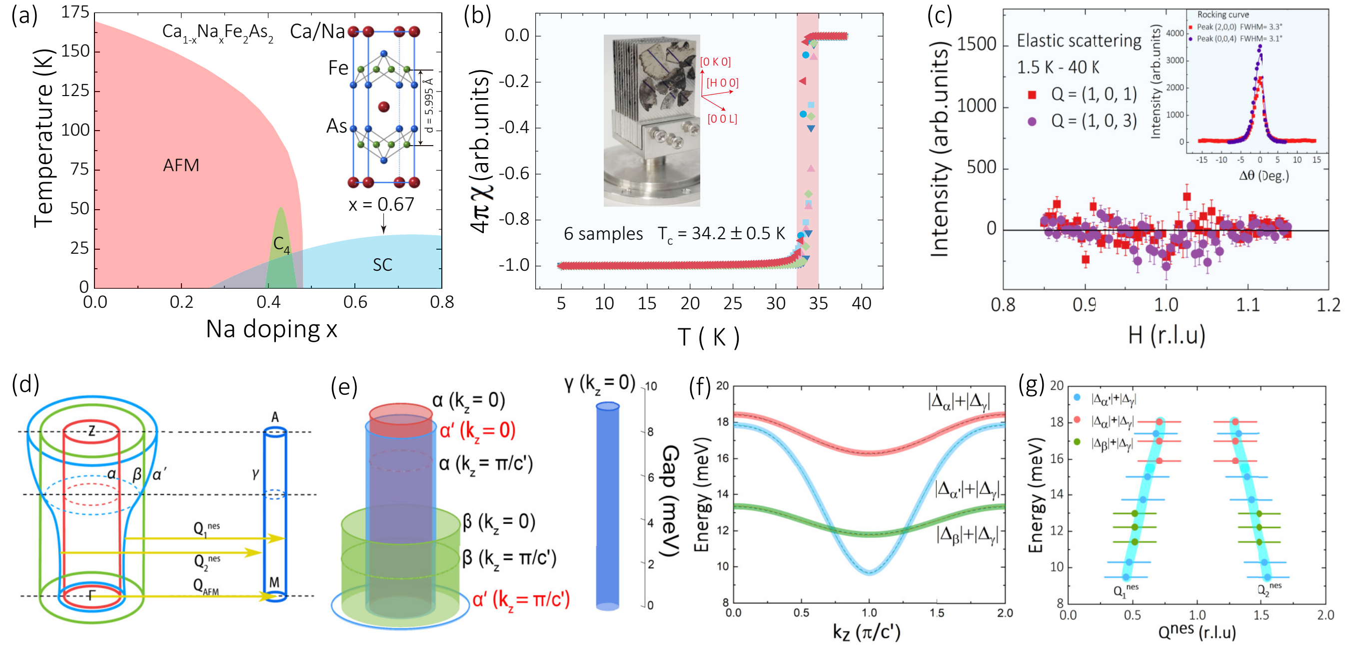

FIG. 1. Sample information, electronic, and magnetic properties of $Ca_{0.33}Na_{0.67}Fe_2As_2$. (a) Phase diagram and crystal structure of $Ca_{1-x}Na_xFe_2As_2$ [94]. The arrow marks the doping level ($x = 0.67$) in this study [74]. (b) Zero-field-cooling magnetization in six randomly selected samples. The average T_c is 34.2 ± 0.5 K. The inset shows the coaligned sample set. (c) Elastic neutron scattering results of the difference between $T = 1.5$ K and $T = 40$ K at $Q = (1, 0, 1)$ and $Q = (1, 0, 3)$. The zero intensity suggests no antiferromagnetic order in this compound. The inset shows the rocking curves and the FWHM for Bragg peaks (2, 0, 0) and (0, 0, 4). (d) Sketch plot of the 3D Fermi surfaces. There are three hole pockets (α, α', β) around the zone center and a small electron pocket (γ) around the zone corner, where α' band shows strongly dispersive behavior along k_z ($\Gamma - Z$) direction [79]. The two different nesting vectors $\mathbf{Q}_{1,2}^{\mathrm{nes}}$ and the antiferromagnetic wave vector in the parent compound ($\mathbf{Q}_{\mathrm{AFM}}$) are marked. (e) Sketch plot of the superconducting gaps on each Fermi sheet at $k_z = 0$ (Γ) and $k_z = \pi/c'$ (Z) [79]. (f) k_z modulation of the total superconducting gaps for each pair of the pockets: $|\Delta_\alpha| + |\Delta_\gamma|$, $|\Delta_{\alpha'}| + |\Delta_\gamma|$, $|\Delta_\beta| + |\Delta_\gamma|$. The dashed lines represent two cases for momentum transfer $Q = (1, 0, L)$ (L = odd or even). (g) Distribution of the total superconducting gaps at two nesting vectors $\mathbf{Q}_{1,2}^{\mathrm{nes}}$ after considering both on the gap value and the pocket size modulations along k_z with selective points.

Theoretical doping was performed within the virtual crystal approximation approach [77]. The GGA plus on-site repulsion U method (GGA + U) was employed to incorporate the associated electron correlation effect. The plane-wave cutoff energy for Kohn-Sham valence states was taken as 50 Ry in all calculations after performing rigourous convergence tests. The Fermi surfaces were calculated using a dense $50 \times 50 \times 50$ k-mesh, and the visualization tool FermiSurfer was used to display the orbital contributions. All five orbitals of Fe^{2+} (d_{xz}, d_{yz}, d_{xy}, d_{z^2}, and $d_{x^2-y^2}$) contribute to the band structure; the partial density of states (PDOS) for each orbital was also derived from the calculation results.

III. RESULTS AND DISCUSSION

The Fermi surfaces of $Ca_{0.33}Na_{0.67}Fe_2As_2$ consist of three hole pockets (α, α', β) and one electron pocket (γ), as shown in previous results of high-resolution angle-resolved photoemission spectroscopy (ARPES) measurements [78,79]. Only the α' band shows a strong modulation along the k_z direction, which appears as the outermost Fermi surface around the Z point [namely, $\mathbf{k} = (0, 0, \pi/c')$, here $c' = c/2$ to represent the distance between two Fe-Fe planes in the 1 Fe/unit cell Brillouin zone], but modulates significantly such that it becomes nearly degenerate with the innermost α band around the Γ point [$\mathbf{k} = (0, 0, 0)$] [Fig. 1(d)]. The γ band is 2D and has a small pocket size both at the M point [$\mathbf{k} = (\pi/a, 0, 0)$] and A point [$\mathbf{k} = (\pi/a, 0, \pi/c')$]. Due to the mismatch of the pocket sizes, the hole and electron pockets are imperfectly nested at two wave vectors $\mathbf{Q}_{1,2}^{\mathrm{nes}} = [1 \pm \delta, 0]$ in fixed k_z plane. While the superconducting gap ($\Delta_{\mathbf{k}}$) is nearly 2D on β and γ bands, it shows a weak k_z modulation from 8 meV to 10 meV on the α band and a very strong k_z modulation from near 0 meV to 8.2 meV on the α' band [Fig. 1(e)]. After considering an interlayer coupling, the gap data on all the bands can be fitted together by using a global gap function: $|\Delta_{\mathbf{k}}| = |\Delta_0 \cos(k_x)\cos(k_y) + \Delta_z[\cos(k_x) + \cos(k_y)]\cos(k_z)/2|$, where $\Delta_0 = 9.9$ meV can be considered as the intralayer pairing gap and $\Delta_z = 1.2$ meV is the interlayer pairing gap [79]. Based on the pocket sizes in the (k_x, k_y) plane at specific k_z positions obtained from ARPES measurements [79], we can calculate the gap value $\Delta_{\mathbf{k}}$ of each band from the above equation. Regardless of the size mismatch, the total superconducting gap for each pair of hole-electron pockets ($|\Delta_\alpha| + |\Delta_\gamma|$, $|\Delta_{\alpha'}| + |\Delta_\gamma|$, $|\Delta_\beta| + |\Delta_\gamma|$) linked by the momentum transfer $Q = (1, 0, L)$ should have a k_z modulation, and they are nearly the same for the cases of L = odd and even [Fig. 1(f)]. By further considering the imperfect Fermi surface nesting, the total gap Δ_{tot} is actually defined by two incommensurate wave vectors $\mathbf{Q}_{1,2}^{\mathrm{nes}}$ varied with the pocket sizes. All the possibilities of Δ_{tot} under different combinations finally form a downward “dispersion” in the

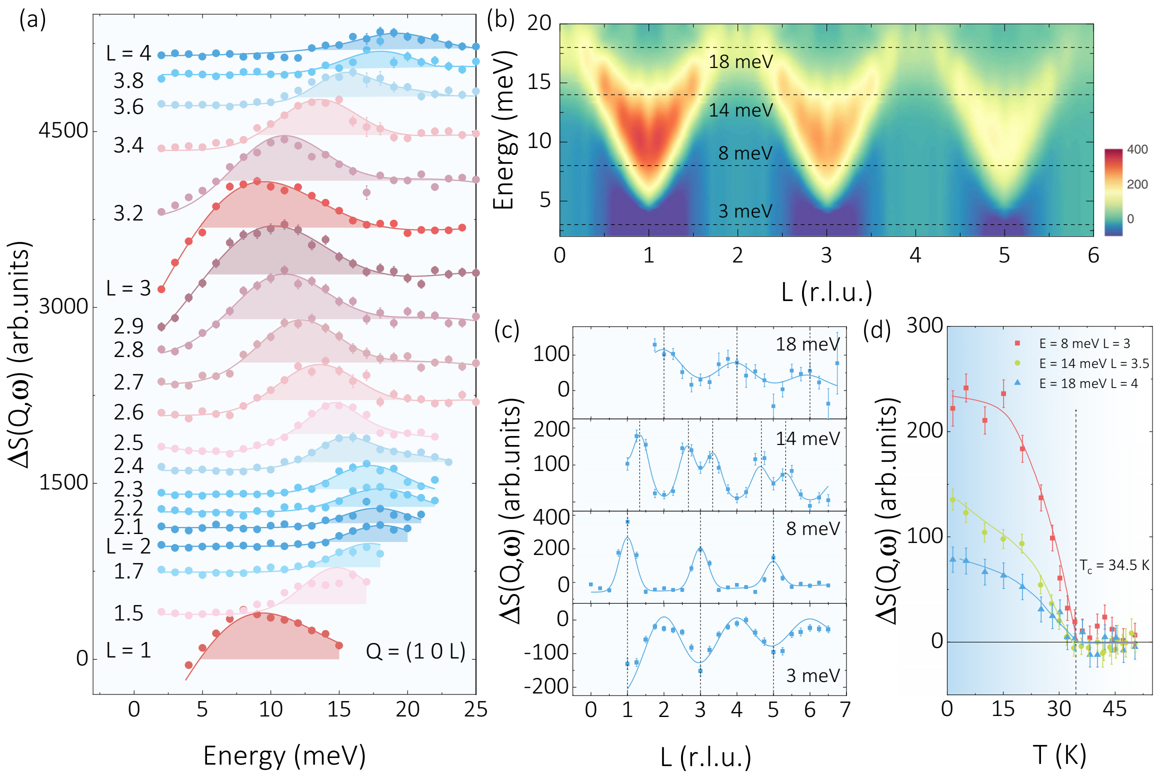

FIG. 2. L dispersion and temperature dependence of the resonance mode as shown by the intensity difference between $T = 1.5$ K and $T = 40$ K. (a) Spin resonance peaks at different $Q = (1, 0, L)(L = 1 \sim 4)$; the intensities have been divided by the square of Fe^{2+} form factor $|F(\mathbf{Q})|^2$. All data are shifted by the steps of L for clarity. (b) 2D color sketch on the L dependence of the spin excitation intensity difference between 1.5 K and 40 K. The horizontal dashed lines in (b) correspond to the 1D L cuts in (c) with $E = 3$, 8, 14, and 18 meV, and the vertical dashed lines in (c) mark the peak positions, respectively. The resonance intensity at high Q is damped due to the form factor effect. (d) Temperature dependence of the resonance intensity at $E = 8$, 14, and 18 meV with $Q = (1, 0, 3)$, (1, 0, 3.5), and (1, 0, 4) respectively. All solid lines are guides to eyes.

momentum space [Fig. 1(g)], where the onset of Δ_{tot} locates near the perfect nesting case with $\mathbf{Q}^{\mathrm{nes}} = \mathbf{Q}_{\mathrm{AFM}}$.

Figures 2(a) and 2(b) present the details of the c-axis dispersion of SRM. After subtracting the intensity of magnetic excitations in the normal state ($T = 40$ K), the SRM in the superconducting state at $T = 1.5$ K can be well identified by a peak in the energy scans at constant $\mathbf{Q}$ positions $\mathbf{Q} = (1, 0, L)(L = 1 \sim 4)$. The SRM has a strong intensity at odd Ls with $E_R = 9.5$ meV (e.g., $L = 1$ and 3), the peak shifts to higher energy and gets weaker from odd Ls to even Ls. For $L = 2$ and 4, $E_R \approx 18$ meV, thus the bandwidth of the c-axis dispersion is about 8.5 meV [Fig. 2(a)]. The V-shape-like c-axis dispersion of the SRM has a velocity $c_L \approx 20$ meVÅ much smaller than the c-axis velocity of spin waves ($\approx$168 meVÅ) in the parent compound [80] [Fig. 2(b)]. To extract the L modulation of the resonance intensity, we have performed long L scans at typical energies at $E = 3$, 8, 14, 18 meV. For the spectral-weight depletion at 3 meV and the intensity gain at 8 meV, they certainly center at odd $L = 1$, 3, 5, while the resonance intensity at 18 meV peaks at even $L = 2$, 4, 6. The L scan at intermediate energy $E = 14$ meV show a two-peak feature instead [Fig. 2(c)]. The intensity gains at $E = 8$ meV, $L = 3$; $E = 14$ meV, $L = 3.5$; and $E = 18$ meV, $L = 4$ show a clear order-parameter-like behavior of the superconductivity below T_c [Fig. 2(d)].

To further explore the dispersion of SRM in the ab plane, we have systematically performed constant-energy scans up to 26 meV along the H direction at three fixed $L = 3$, 3.5, 4, as summarized in Fig. 3. To remove the contamination of phonon excitations, here we only show the intensity difference between 1.5 K and 40 K to refer to the SRM. The in-plane dispersion of SRM can be obtained by Gaussian fitting (double or single peak) on the raw data in Figs. 3(a)–3(c). The peak centers and intensities obtained from these fittings are shown by the open circles and gradient color in Figs. 3(d)–3(f), respectively. For comparison, the momentum distribution of Δ_{tot} in Fig. 1(g) and the L positions in the L dispersion obtained from Fig. 2(a) are also plotted in Figs. 3(b), 3(e), and 3(f), respectively. Similar to other 122-type FeSCs [23,37–40], the in-plane dispersion of SRM is nearly linear in V shape. Assuming the SRM is an in-gap spin exciton under $s^{\pm}$-pairing symmetry, its in-plane dispersion should be in the form of gapped magnons with upward dispersion: $\Omega = \sqrt{\Omega_0^2 + c_H^2 q^2}$, where Ω_0 is the resonance energy at zone center $H = (1, 0)$, and c_H is the spin velocity at $q = 2\pi|(H - 1)|/a$ [37,40]. The fitting of the above equation gives $c_H = 75.2$, 78.5, and 119.2 meVÅ for $L = 3$, 3.5, and 4, respectively. Comparing to the velocity of c-axis dispersion, we have $c_H/c_L = 3.8 \sim 6.0$. The in-plane spin velocity of SRM in $Ca_{0.33}Na_{0.67}Fe_2As_2$ is close to the case in another optimally hole-doped compound

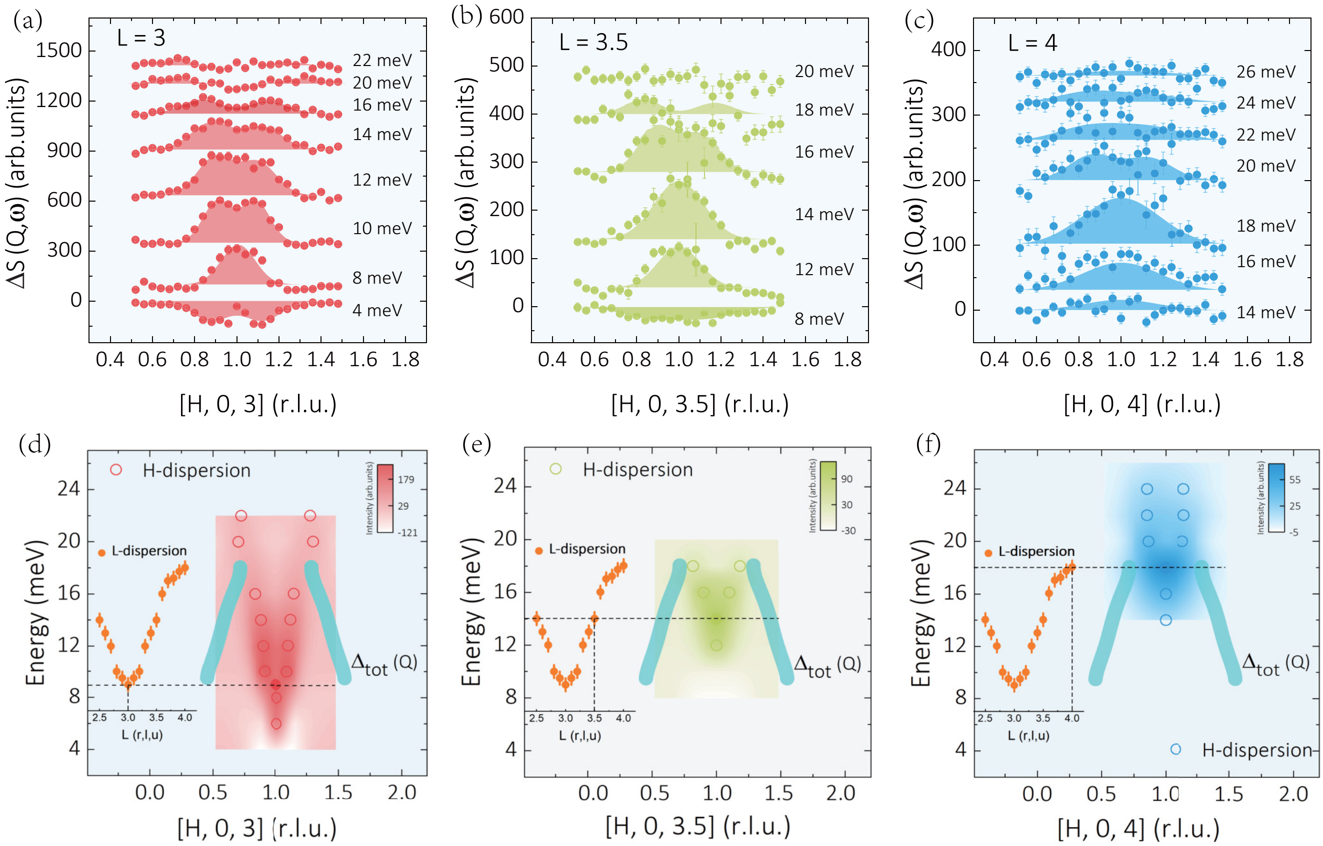

FIG. 3. *H* dispersion of the spin resonance and comparison with $\Delta_{\mathrm{tot}}(\mathbf{Q})$. (a)–(c) Constant-energy scans of the intensity difference between $T = 1.5$ K and $T = 40$ K along the $[H, 0, L]$ direction at various transfer energies with fixed $L = 3$, 3.5, and 4, respectively. The shade areas are fitting results by a one-Gaussian-peak or two-Gaussian-peak function. All data are shifted for clarity. (d)–(f) Comparison between the *H* dispersion of the spin resonance and the momentum distribution of $\Delta_{\mathrm{tot}}(\mathbf{Q})$ obtained from Fig. 1(f). The color map and open circles represent the resonance dispersions and peak positions, respectively. The dashed lines mark the peak energy E_R and the *L* position in the *L* dispersion shown by insets.

$Ba_{0.67}K_{0.33}Fe_2As_2$, even though the latter compound has very weak *c*-axis dispersion of SRM [40]. The comparable spin velocity between the cases along the *c* axis and in the *ab* plane confirms the 3D nature of SRM in $Ca_{0.33}Na_{0.67}Fe_2As_2$, and the SRM becomes harder when it disperses to higher energy at even *L*s. We also notice that the *c* axis to in-plane ratio of spin velocity for the spin waves in $CaFe_2As_2$ is about 1.9 [80], much smaller than the case in SRM of $Ca_{0.33}Na_{0.67}Fe_2As_2$. Thus, the 3D dispersion of SRM cannot been fully attributed to the damped magnetic excitations in the normal state, which are similar to the spin-wave dispersions in parent compounds due to the nearly unchanged effective magnetic coupling *J* [9,80–82]. From another perspective, the upward in-plane dispersion of SRM apparently does not follow the downward distribution of Δ_{tot}. The overall intensity of SRM may be confined by the maximum gap for $L = 3$ and 3.5 within the energy resolutions in our measurements, but definitely break through the limitation of Δ_{tot} for the $L = 4$ case, where E_R is nearly identical to the onset of Δ_{tot}. Such results are also observed in other hole-doped compounds such as $Ba_{0.67}K_{0.33}Fe_2As_2$ and (K, Cs)$Ca_2Fe_4As_4F_2$, which is actually inconsistent with the spin exciton scenario and require further theoretical investigations [32,33,40,70,83–85].

From the global gap function, it illustrates that the k_z modulation of the gap is mostly from the pocket size change under the interlayer pairing ($\Delta_z \neq 0$) [79]. Such a picture is experimentally confirmed in $Ba_{1-x}(K, Na)_xFe_2As_2$ and $BaFe_2(As_{1-x}P_x)_2$ [63,70]. To further reveal the orbital contributions on each Fermi surface, we have performed DFT calculations on $Ca_{0.33}Na_{0.67}Fe_2As_2$; the results are shown in Fig. 4. Clearly, all five orbitals of Fe^{2+} (d_{xz}, d_{yz}, d_{xy}, d_{z^2} and $d_{x^2-y^2}$) contribute to the Fermi surfaces, and the pocket size modulation is highly related to the PDOS of each orbital [Figs. 4(a)–4(e)]. For the strongly modulated α' band, only the d_{xz} and d_{z^2} orbitals follow the modulation period both on size and gap [Figs. 4(f)–4(j)]. This could be further confirmed by the orbital projected Fermi surfaces in 3D [Figs. 4(k)–4(o)]. However, the modulation amplitude for d_{z^2} orbital is obviously higher than that in d_{xz} orbital. By integrating the occupation of all Fermi surfaces for each orbital, it emphasizes the importance of d_{z^2} orbital in total DOS [Fig. 5(a)], as its peak is very close to the Fermi level. Even though the PDOS is dominated by d_{xz}, d_{yz}, and $d_{x^2-y^2}$, the k_z modulation of d_{z^2} orbital is quite obvious [Fig. 5(b)]. It seems that the more involvement of d_{z^2} to the Fermi level, yields the larger size of the pocket and the smaller superconducting gap. This

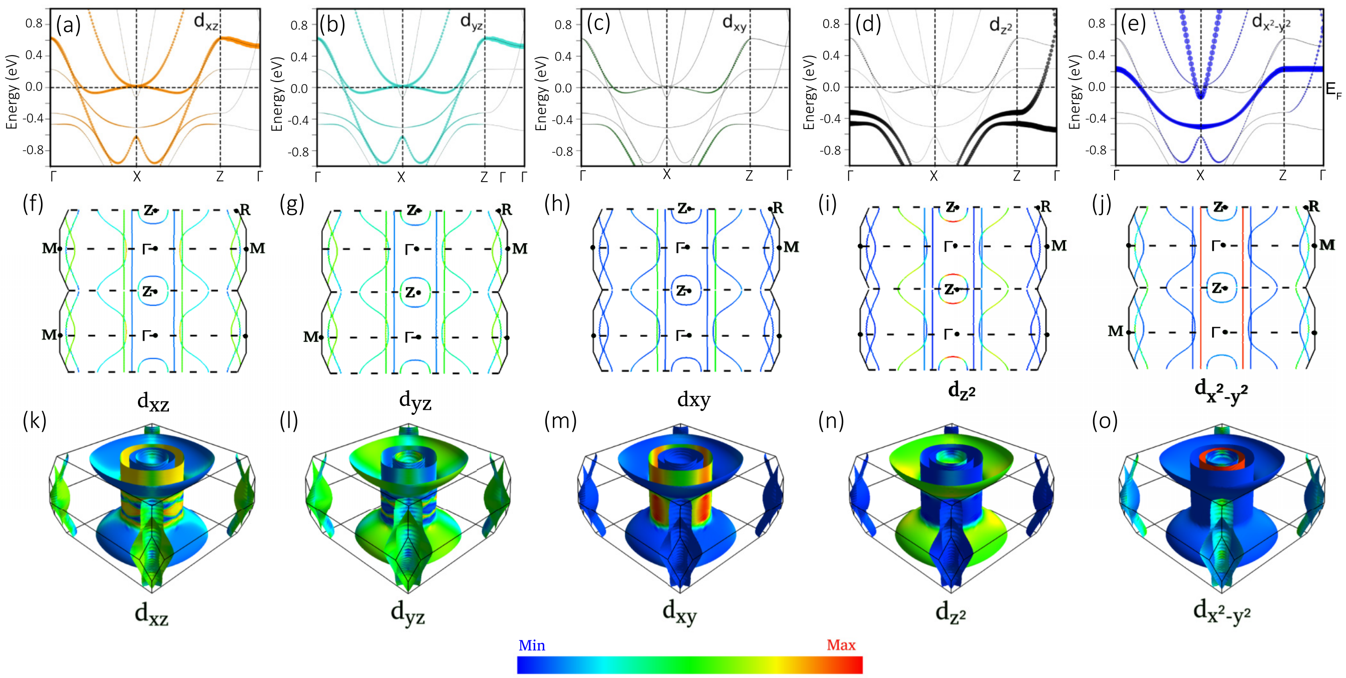

FIG. 4. Occupation for five Fe^{2+} orbitals in the band structure and each Fermi sheet obtained from DFT calculations. (a)–(e) Occupation in band structure for five Fe^{2+} orbitals (d_{xz}, d_{yz}, d_{xy}, d_{z^2}, and $d_{x^2-y^2}$). The size of dots represent the PDOS for each orbital. (f)–(j) k_z modulation of PDOS in 2D for all five Fe^{2+} orbitals. (k)–(o) Orbital projected Fermi surfaces in 3D for all five Fe^{2+} orbitals. The gradient colors from blue to red represent the relative intensities.

naturally establishes the connection between the Fe-As layer distance d and the k_z modulation of superconducting gap. When two Fe-As layers get closer, the interlayer overlap of d_{z^2} orbital is more likely to happen. Such effect is significant in those compounds with mirror symmetric Fe-As layers along c axis under short d (e.g., the 122-type or 1144-type FeSCs) [Fig. 5(c)], since the possible hybridization between the $4p_z$ orbital of As and the d_{z^2} orbital of Fe could enhance the interlayer coupling [86,87].

The above facts inspire us to search for the possible connections between the c-axis resonance dispersion and the distance of adjacent Fe-As layers (d). The c-axis dispersion of SRM can be quantitatively described by the bandwidth $\Delta E = E_{\text{even}} - E_{\text{odd}}$, namely, the peak energy difference between even and odd Ls [36]. To compare with different systems near the optimal doping level, we have normalized ΔE by $k_B T_c$, and then plot it versus d for all available data in iron-pnictide superconductors [24–26,29–32,34–41]. As shown in Fig. 5(d), it turns out that c-axis bandwidth of SRM has a universal scaling relationship with d. For those systems with large d, such as 12442, 111, 112, and 10-3-8, the SRM is 2D with $\Delta E = 0$ [26,31,32]. When d decreases below a threshold of about 6.7 Å, the c-axis dispersion of SRM appears and continuously increases along with further decreasing d. Similar scaling can be also found for the intensity ratio $I_{\text{odd}}/I_{\text{even}}$, as the resonance at even L is always weaker than that at odd L [Fig. 5(e)]. Interestingly, for the bilayer compound $CaKFe_4As_4$ with breaking translation symmetry along the c axis, the SRM splits into nondispersive odd and even modes instead of the continuous c-axis dispersion [34], it also follows the same scaling with the shortest d in Figs. 5(d) and 5(e), too. Therefore, the Fe-As layer distance d plays a key role in the c-axis dispersion of SRM. To further seek the relation between d and the k_z modulation of superconducting gaps, herein we compare the available ARPES results of four compounds: $Ba_{0.6}Na_{0.4}Fe_2As_2$, $BaFe_2(As_{0.66}P_{0.34})_2$, $Ba_{0.67}K_{0.33}Fe_2As_2$, and $Ca_{0.33}Na_{0.67}Fe_2As_2$ in this paper [36,41,69,70,79,83,84]. Since most bands have nearly 2D gaps, we thus only focus on the k_z modulation of gap of the α' band: $[\Delta_{\alpha'}(0) - \Delta_{\alpha'}(\pi/c')]/k_B T_c$. Not surprisingly, the k_z modulation of the gap is also anticorrelated with the Fe-As layer distance [Fig. 5(f)], but weaker than the scaling of the c-axis dispersion of SRM in Fig. 5(d). Such results clearly confirm the common nature of the 3D dispersions of SRM and the superconducting gaps.

The threshold of $d = 6.7$ Å divides the FeSCs into two groups: the weak coupled systems with $d > 6.7$ Å and the strong coupled systems with $d < 6.7$ Å. On one hand, the dispersion of SRM is determined by the nesting conditions and the gap distributions on the Fermi surfaces of the weak coupled systems, as the magnetic excitations are dominated by the contributions from itinerant electrons. On the other hand, it could keep the "memory" of magnons in those strong coupled systems, as the magnetic excitations are mainly contributed by local magnetic moments. Therefore, the dispersion of SRM could either show a downward feature in quasi-2D systems (e.g., $KCa_2Fe_4As_4F_2$) or an upward feature in 3D systems (e.g., $Ca_{1-x}Na_xFe_2As_2$). When the SRM is strong enough, the magnetic excitation changes (ΔE_{ex}) below and above T_c should account for the superconducting condensation energy (U_c), namely, $\Delta E_{\text{ex}}/U_c \gg 1$ [38,82]. It seems that the magnetic system is easier to resonate with the superconductivity under shorter d due to the enhanced interlayer coupling. In this sense, the interlayer pairing in FeSCs could also be driven

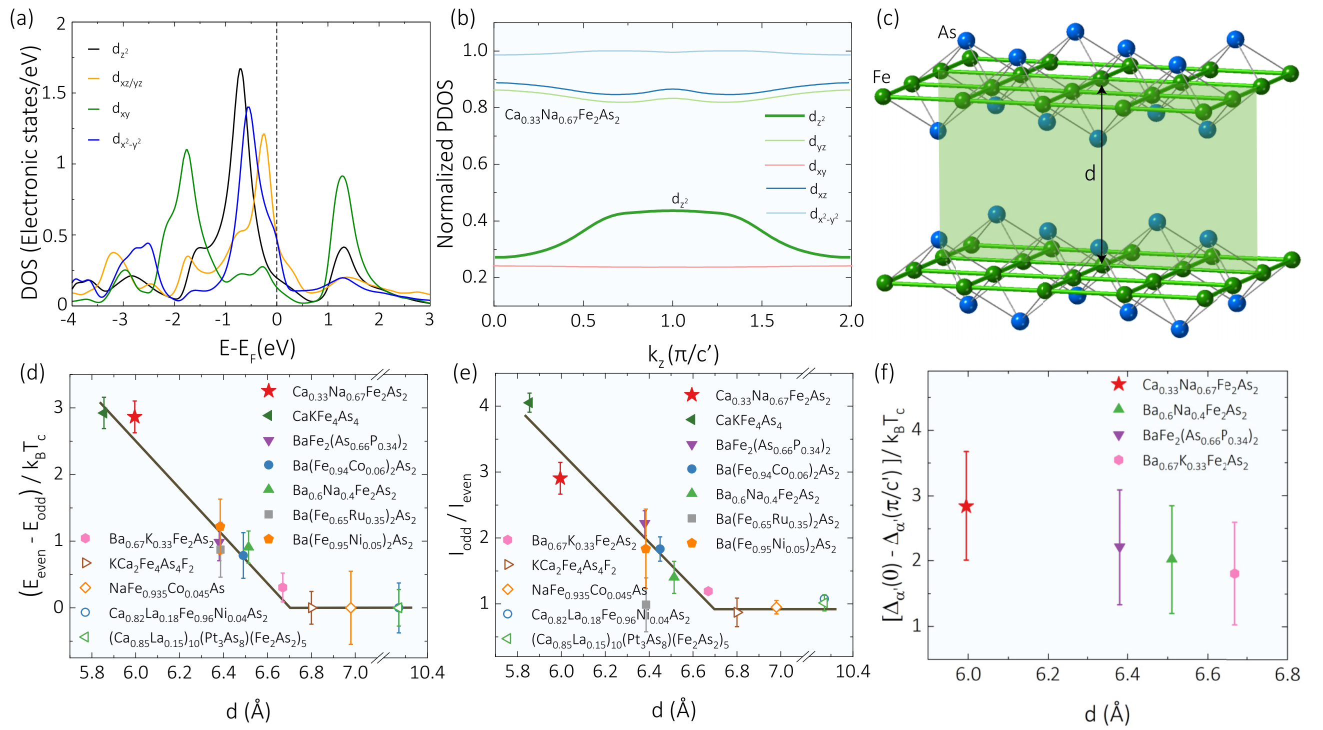

FIG. 5. Analysis of density of states, c-axis resonance dispersion, superconducting gap modulation, and Fe-As interlayer distance in iron-pnictide superconductors. (a) The total DOS for all five Fe^{2+} orbitals obtained from DFT calculations. (b) k_z modulation of the normalized PDOS for all five Fe^{2+} orbitals derived from DFT calculations. (c) The distance of adjacent Fe-As layers d in iron-pnictide superconductors. (d), (e) Universal relationship between the c-axis resonance dispersion and the Fe-As interlayer distance d in iron-pnictide superconductors. The bandwidth of resonance ($E_{\mathrm{even}} - E_{\mathrm{odd}}$) is normalized by $k_B T_c$, and the intensity ratio $I_{\mathrm{odd}}/I_{\mathrm{even}}$ is obtained from the energy scans at $Q = (1, 0, L)$ [24–26,29,31,32,34–41]. The solid lines are guides to the eyes. (f) Anticorrelation between the k_z gap modulation of α' band and the Fe-As layer distance in four compounds: $Ba_{0.6}Na_{0.4}Fe_2As_2$, $BaFe_2(As_{0.66}P_{0.34})_2$, $Ba_{0.67}K_{0.33}Fe_2As_2$, and $Ca_{0.33}Na_{0.67}Fe_2As_2$ [36,40,41,70,79,83,84].

by magnetic fluctuations similar to the intralayer pairing but involved with different orbital contributions (i.e., d_{z^2} orbital). This picture is also supported by a commonly observed feature of c-axis preferred SRM for different magnetic patterns [41,87–91], suggesting orbital-selective pairings in FeSCs.

Theoretically, the intra- and interlayer pairings generally compete with each other and can be tuned by the local magnetic interactions related to the in-plane correlations and the Fe-As layer distance [86]. This picture naturally explains the rich superconducting phase induced by various chemical substitutions in FeSCs. While the in-plane substitutions of Fe by other transition metals (e.g., Ni, Co, Ru, Rh,...) break the static AFM orders and establish the intralayer pairing, the out-of-plane substitutions (e.g., Na, K. Rb, Cs,...) stretch the c axis to reduce interlayer coupling, and the isovalent doping from P on As sites actually decreases the average pnictogen height to give a smaller d [2,3,9,38,56,57]. The superconductivity is not solely determined by the charge carrier concentration from dopings but also highly related to the additional effects from local crystalline structures. Therefore, the bilayer compounds with strong interlayer couplings do not always have higher T_c than the single layer compounds [11,57–61,92], and the optimal doping level is compound dependent even for those systems with same lattice symmetry and chemical substitution [e.g., optimal doping level $x = 0.4$, 0.55, and 0.67 for $Ba_{1-x}Na_xFe_2As_2$ ($d \approx 6.5$ Å), $Sr_{1-x}Na_xFe_2As_2$ ($d \approx 6.2$ Å), $Ca_{1-x}Na_xFe_2As_2$ ($d \approx 5.9$ Å), respectively] [74,93–98]. This also explains why the Fe-As-Fe bond angle as well as the anion height from the Fe-Fe plane are related to the optimal T_c in different FeSCs [3,99,100], since they directly relate to the Fe-As layer distance.

IV. SUMMARY

In summary, our INS experiment reveals a 3D neutron SRM in the superconducting state of $Ca_{0.33}Na_{0.67}Fe_2As_2$ with upward V-shape dispersions both in the Fe-As plane and along the c axis. The in-plane dispersion of SRM does not follow the energy-momentum distribution of the total supeconducting gap Δ_{tot} summed on those imperfectly nesting Fermi sheets with k_z modulations. By comparing with other FeSCs, we demonstrate that the c-axis dispersion of SRM can be universally scaled with the Fe-As layer distance d, and the k_z-modulation of gap is also anticorrelated with d. The threshold of $d = 6.7$ Å divides the FeSCs into two groups with different interlayer coupling, which determines the dimensionality of superconductivity and SRM. The competition between the intra- and interlayer pairings leads to the tunable and flexible superconductivity in FeSCs, but probably limits the maximum T_c in these materials. Therefore, the common picture of a doped Mott insulator in cuprates may not be applicable in the metallic FeSCs [1,2], as their multiband superconductivity is more sensitive to the local crystalline parameters besides charge dopings. Further investigations on the quantitative relationship between the local structure and T_c in FeSCs will certainly inspire the quest for a universal mechanism of the magnetically driven picture of high-T_c superconductivity.

ACKNOWLEDGMENTS

This work is supported by the National Key Research and Development Program of China (Grants No. 2018YFA0704200, No. 2022YFA1403400, and No. 2021YFA1400400), the National Natural Science Foundation of China (Grants No. 11822411, No. 11961160699, No. 11974392, and No. 12061130200), the Strategic Priority Research Program (B) of the CAS (Grants No. XDB25000000 and No. XDB33000000) and K. C. Wong Education Foundation (No. GJTD-2020-01). H.L. is grateful for the support from the Youth Innovation Promotion Association of CAS (Grant No. Y202001) and Beijing Natural Science Foundation (Grant No. JQ19002). W.H. acknowledges support from the Postdoctoral Innovative Talent program (No. BX2021018) and the China Postdoctoral Science Foundation (No. 2021M700250). A.P. acknowledges the Homi Bhaba National Institute at Raja Ramanna Centre for Advanced Technology. This work is based on neutron scattering experiments performed at the Swiss Spallation Neutron Source (SINQ), Paul Scherrer Institut, Villigen, Switzerland (Proposals No. 20202218 and No. 20210956).

W.H., H.Z., Z.L., and Y.L. grew the crystals of $Ca_{0.33}Na_{0.67}Fe_2As_2$ and did the sample characterizations. W.H., H.Z., Z.L., Y.L., Z.T., and X.L. coaligned the crystals. W.H., H.L., H. Z., Z.L., and U.S. performed the neutron scattering experiments. W.H., S.L., and H.L. analyzed the data. H.G. and A.P. did the DFT calculations. J.H. gave theoretical suggestions. H.L., W.H., H.G., and S.L. wrote the paper. The project was supervised by H.L. All authors discussed the results, interpretation, and conclusion.

[1] P. A. Lee, N. Nagaosa, and X.-G. Wen, Doping a Mott insulator: Physics of high-temperature superconductivity, Rev. Mod. Phys. **78**, 17 (2006).

[2] Q. Si, R. Yu, and E. Abrahams, High-temperature superconductivity in iron pnictides and chalcogenides, Nat. Rev. Mater. **1**, 16017 (2016).

[3] X. Chen, P. Dai, D. Feng, T. Xiang, and F. C. Zhang, Iron-based high transition temperature superconductors, Nat. Sci. Rev. **1**, 371 (2014).

[4] X. Zhou, W. S. Lee, M. Imada, N. Trivedi, P. Phillips, H. Y. Kee, P. Törmä, and M. Eremets, High-temperature superconductivity, Nat. Rev. Phys. **3**, 462 (2021).

[5] Q. Gu and H. H. Wen, Superconductivity in nickel-based 112 systems, The Innovation **3**, 100202 (2022).

[6] B. D. White, J. D. Thompson, and M. B. Maple, Unconventional superconductivity in heavy-fermion compounds, Phys. C: Supercond. **514**, 246 (2015).

[7] X. Zhong, J. S. Tse, R. J. Hemley, and H. Liu, Theory-directed discovery of high-temperature superconductivity in clathrate hydrides at high pressure, The Innovation **3**, 100226 (2022).

[8] J. M. Tranquada, G. Xu, and I. A. Zaliznyak, Superconductivity, antiferromagnetism, and neutron scattering, J. Magn. Magn. Mater. **350**, 148 (2014).

[9] P. Dai, Antiferromagnetic order and spin dynamics in iron-based superconductors, Rev. Mod. Phys. **87**, 855 (2015).

[10] J. Paglione and R. L. Greene, High-temperature superconductivity in iron-based materials, Nat. Phys. **6**, 645 (2010).

[11] D. C. Johnston, The puzzle of high temperature superconductivity in layered iron pnictides and chalcogenides, Adv. Phys. **59**, 803 (2010).

[12] J. Rossat-Mignod, L. P. Regnault, C. Vettier, P. Bourges, P. Burlet, J. Bossy, J. Y. Henry, and G. Lapertot, Neutron scattering study of the $YBa_2Cu_3O_{6+x}$ system, Phys. C: Supercond. **185**, 86 (1991).

[13] D. J. Scalapino, A common thread: The pairing interaction for unconventional superconductors, Rev. Mod. Phys. **84**, 1383 (2012).

[14] Y. Sidis, S. Pailhès, V. Hinkov, B. Fauqué, C. Ulrich, L. Capogna, A. Ivanov, L.-P. Regnault, B. Keimer, and P. Bourges, Inelastic neutron scattering study of spin excitations in the superconducting state of high temperature superconductors, C. R. Phys. **8**, 745 (2007).

[15] P. D. Johnson, G. Xu, and W. Yin, *Iron-based Superconductivity* (Springer, New York, 2015), pp. 165–169.

[16] A. D. Christianson, E. A. Goremychkin, R. Osborn, S. Rosenkranz, M. D. Lumsden, C. D. Malliakas, I. S. Todorov, H. Claus, D. Y. Chung, M. G. Kanatzidis, R. I. Bewley, and T. Guidi, Unconventional superconductivity in $Ba_{0.6}K_{0.4}Fe_2As_2$ from inelastic neutron scattering, Nature (London) **456**, 930 (2008).

[17] D. Gong and H. Luo, Antiferromagnetic order and spin dynamics in iron-based superconductors, Acta Phys. Sin. **67**, 207407 (2018).

[18] H. Luo, Neutron scattering studies on the magnetic interaction in iron-based superconductor $BaFe_{2-x}Ni_xAs_2$ (in Chinese), Chin. Sci. Bull. **62**, 3955 (2017).

[19] Y. Qiu, W. Bao, Y. Zhao, C. Broholm, V. Stanev, Z. Tesanovic, Y. C. Gasparovic, S. Chang, J. Hu, B. Qian, M. Fang, and Z. Mao, Spin Gap and Resonance at the Nesting Wave Vector in Superconducting $FeSe_{0.4}Te_{0.6}$, Phys. Rev. Lett. **103**, 067008 (2009).

[20] D. S. Inosov, J. T. Park, P. Bourges, D. L. Sun, Y. Sidis, A. Schneidewind, K. Hradil, D. Haug, C. T. Lin, B. Keimer, and V. Hinkov, Normal-state spin dynamics and temperature-dependent spin-resonance energy in optimally doped $BaFe_{1.85}Co_{0.15}As_2$, Nat. Phys. **6**, 178 (2010).

[21] T. J. Liu, J. Hu, B. Qian, D. Fobes, Z. Q. Mao, W. Bao, M. Reehuis, S. A. J. Kimber, K. Prokes, S. Matas, D. N. Argyriou, A. Hiess, A. Rotaru, H. Pham, L. Spinu, Y. Qiu, V. Thampy, A. T. Savici, J. A. Rodriguez, and C. Broholm, From (π, 0) magnetic order to superconductivity with (π, π) magnetic resonance in $Fe_{1.02}Te_{1-x}Se_x$, Nat. Mater. **9**, 718 (2010).

[22] H. Luo, M. Wang, C. Zhang, X. Lu, L.-P. Regnault, R. Zhang, S. Li, J. Hu, and P. Dai, Spin Excitation Anisotropy as a Probe of Orbital Ordering in the Paramagnetic Tetragonal Phase of Superconducting $BaFe_{1.904}Ni_{0.096}As_2$, Phys. Rev. Lett. **111**, 107006 (2013).

[23] H. Luo, X. Lu, R. Zhang, M. Wang, E. A. Goremychkin, D. T. Adroja, S. Danilkin, G. Deng, Z. Yamani, and P. Dai, Electron doping evolution of the magnetic excitations in $BaFe_{2-x}Ni_xAs_2$, Phys. Rev. B **88**, 144516 (2013).

[24] C. Zhang, M. Wang, H. Luo, M. Wang, M. Liu, J. Zhao, D. L. Abernathy, T. A. Maier, K. Marty, M. D. Lumsden, S. Chi, S. Chang, J. A. Rodriguez-Rivera, J. W. Lynn, T. Xiang, J. Hu, and P. Dai, Neutron scattering studies of spin excitations in hole-doped $Ba_{0.67}K_{0.33}Fe_2As_2$ superconductor, Sci. Rep. **1**, 115 (2011).

[25] J. Zhao, C. R. Rotundu, K. Marty, M. Matsuda, Y. Zhao, C. Setty, E. Bourret-Courchesne, J. Hu, and R. J. Birgeneau, Effect of Electron Correlations on Magnetic Excitations in the Isovalently Doped Iron-Based Superconductor $Ba(Fe_{1-x}Ru_x)_2As_2$, Phys. Rev. Lett. **110**, 147003 (2013).

[26] C. Zhang, H.-F. Li, Y. Song, Y. Su, G. Tan, T. Netherton, C. Redding, S. V. Carr, O. Sobolev, A. Schneidewind, E. Faulhaber, L. W. Harriger, S. Li, X. Lu, D.-X. Yao, T. Das, A. V. Balatsky, Th. Brückel, J. W. Lynn, and P. Dai, Distinguishing $s_\pm$ and s_{++} electron pairing symmetries by neutron spin resonance in superconducting $NaFe_{0.935}Co_{0.045}As$, Phys. Rev. B **88**, 064504 (2013).

[27] Q. Wang, Y. Shen, B. Pan, Y. Hao, M. Ma, F. Zhou, P. Steffens, K. Schmalzl, T. R. Forrest, M. Abdel-Hafiez, X. Chen, D. A. Chareev, A. N. Vasiliev, P. Bourges, Y. Sidis, H. Cao, and J. Zhao, Strong interplay between stripe spin fluctuations, nematicity and superconductivity in FeSe, Nat. Mater. **15**, 159 (2016).

[28] M. Ma, L. Wang, P. Bourges, Y. Sidis, S. Danilkin, and Y. Li, Low-energy spin excitations in $(Li_{0.8}Fe_{0.2})ODFeSe$ superconductor studied with inelastic neutron scattering, Phys. Rev. B **95**, 100504(R) (2017).

[29] M. Wang, H. Luo, J. Zhao, C. Zhang, M. Wang, K. Marty, S. Chi, J. W. Lynn, A. Schneidewind, S. Li, and P. Dai, Electron-doping evolution of the low-energy spin excitations in the iron arsenide superconductor $BaFe_{2-x}Ni_xAs_2$, Phys. Rev. B **81**, 174524 (2010).

[30] J. T. Park, D. S. Inosov, A. Yaresko, S. Graser, D. L. Sun, P. Bourges, Y. Sidis, Y. Li, J.-H. Kim, D. Haug, A. Ivanov, K. Hradil, A. Schneidewind, P. Link, E. Faulhaber, I. Glavatskyy, C. T. Lin, B. Keimer, and V. Hinkov, Symmetry of spin excitation spectra in the tetragonal paramagnetic and superconducting phases of 122-ferropnictides, Phys. Rev. B **82**, 134503 (2010).

[31] T. Xie, D. Gong, H. Ghosh, A. Ghosh, M. Soda, T. Masuda, S. Itoh, F. Bourdarot, L.-P. Regnault, S. Danilkin, S. Li, and H. Luo, Neutron Spin Resonance in the 112-Type Iron-Based Superconductor, Phys. Rev. Lett. **120**, 137001 (2018).

[32] W. Hong, L. Song, B. Liu, Z. Li, Z. Zeng, Y. Li, D. Wu, Q. Sui, T. Xie, S. Danilkin, H. Ghosh, A. Ghosh, J. Hu, L. Zhao, X. Zhou, X. Qiu, S. Li, and H. Luo, Neutron Spin Resonance in a Quasi-two-Dimensional Iron-Based Superconductor, Phys. Rev. Lett. **125**, 117002 (2020).

[33] D. T. Adroja, S. J. Blundell, F. Lang, H. Luo, Z. Wang, and G. Cao, Observation of a neutron spin resonance in the bilayered superconductor $CsCa_2Fe_4As_4F_2$, J. Phys.: Condens. Matter **32**, 435603 (2020).

[34] T. Xie, Y. Wei, D. Gong, T. Fennell, U. Stuhr, R. Kajimoto, K. Ikeuchi, S. Li, J. Hu, and H. Luo, Odd and Even Modes of Neutron Spin Resonance in the Bilayer Iron-Based Superconductor $CaKFe_4As_4$, Phys. Rev. Lett. **120**, 267003 (2018).

[35] P. Steffens, C. H. Lee, N. Qureshi, K. Kihou, A. Iyo, H. Eisaki, and M. Braden, Splitting of Resonance Excitations in Nearly Optimally Doped $Ba(Fe_{0.94}Co_{0.06})_2As_2$: An Inelastic Neutron Scattering Study with Polarization Analysis, Phys. Rev. Lett. **110**, 137001 (2013).

[36] C. H. Lee, P. Steffens, N. Qureshi, M. Nakajima, K. Kihou, A. Iyo, H. Eisaki, and M. Braden, Universality of the Dispersive Spin-Resonance Mode in Superconducting $BaFe_2As_2$, Phys. Rev. Lett. **111**, 167002 (2013).

[37] M. G. Kim, G. S. Tucker, D. K. Pratt, S. Ran, A. Thaler, A. D. Christianson, K. Marty, S. Calder, A. Podlesnyak, S. L. Budko, P. C. Canfield, A. Kreyssig, A. I. Goldman, and R. J. McQueeney, Magnonlike Dispersion of Spin Resonance in Ni-Doped $BaFe_2As_2$, Phys. Rev. Lett. **110**, 177002 (2013).

[38] D. Hu, Z. Yin, W. Zhang, R. A. Ewings, K. Ikeuchi, M. Nakamura, B. Roessli, Y. Wei, L. Zhao, G. Chen, S. Li, H. Luo, K. Haule, G. Kotliar, and P. Dai, Spin excitations in optimally P-doped $BaFe_2(As_{0.7}P_{0.3})_2$ superconductor, Phys. Rev. B **94**, 094504 (2016).

[39] R. Zhang, W. Wang, T. A. Maier, M. Wang, M. B. Stone, S. Chi, B. Winn, and P. Dai, Neutron spin resonance as a probe of Fermi surface nesting and superconducting gap symmetry in $Ba_{0.67}K_{0.33}(Fe_{1-x}Co_x)_2As_2$, Phys. Rev. B **98**, 060502(R) (2018).

[40] T. Xie, C. Liu, T. Fennell, U. Stuhr, S. Li, and H. Luo, Dispersion of neutron spin resonance mode in $Ba_{0.67}K_{0.33}Fe_2As_2$, Chin. Phys. B **30**, 127402 (2021).

[41] F. Waßer, J. T. Park, S. Aswartham, S. Wurmehl, Y. Sidis, P. Steffens, K. Schmalzl, B. Büchner, and M. Braden, Strong spin resonance mode associated with suppression of soft magnetic ordering in hole-doped $Ba_{1-x}Na_xFe_2As_2$, npj Quantum Mater. **4**, 59 (2019).

[42] M. Eschrig, The effect of collective spin-1 excitations on electronic spectra in high-T_c superconductors, Adv. Phys. **55**, 47 (2006).

[43] A. V. Chubukov, D. V. Efremov, and I. Eremin, I., Magnetism, superconductivity, and pairing symmetry in iron-based superconductors, Phys. Rev. B **78**, 134512 (2008).

[44] M. M. Korshunov and I. Eremin, Theory of magnetic excitations in iron-based layered superconductors, Phys. Rev. B **78**, 140509(R) (2008).

[45] T. A. Maier and D. J. Scalapino, Phys. Rev. B **78**, 020514(R) (2008).

[46] T. A. Maier, S. Graser, D. J. Scalapino, and P. Hirschfeld, Neutron scattering resonance and the iron-pnictide superconducting gap, Phys. Rev. B **79**, 134520 (2009).

[47] T. Das, and A. V. Balatsky, Two Energy Scales in the Magnetic Resonance Spectrum of Electron and Hole Doped Pnictide Superconductors, Phys. Rev. Lett. **106**, 157004 (2011).

[48] G. Yu, Y. Li, E. M. Motoyama, and M. Greven, A universal relationship between magnetic resonance and superconducting gap in unconventional superconductors, Nat. Phys. **5**, 873 (2009).

[49] D. S. Inosov, J. T. Park, A. Charnukha, Y. Li, A. V. Boris, B. Keimer, and V. Hinkov, Crossover from weak to strong pairing in unconventional superconductors, Phys. Rev. B **83**, 214520 (2011).

[50] Y. J. Uemura, L. P. Le, G. M. Luke, B. J. Sternlieb, W. D. Wu, J. H. Brewer, T. M. Riseman, C. L. Seaman, M. B. Maple, M. Ishikawa, D. G. Hinks, J. D. Jorgensen, G. Saito, and H. Yamochi, Basic Similarities Among Cuprate, Bismuthate, Organic, Chevrel-Phase, and Heavy-Fermion Superconductors Shown by Penetration-depth Measurements, Phys. Rev. Lett. **66**, 2665 (1991).

[51] R. J. Cava, Oxide superconductors, J. Am. Ceram. Soc. **83**, 5 (2000).

[52] N. Barišić, M. K. Chan, Y. Li, G. Yu, X. Zhao, M. Dressel, A. Smontara, and M. Greven, Universal sheet resistance and revised phase diagram of the cuprate high-temperature superconductors, Proc. Natl. Acad. Sci. USA **110**, 12235 (2013).

[53] A. Iyo, Y. Tanaka, H. Kito, Y. Kodama, P. M. Shirage, D. D. Shivagan, H. Matsuhata, K. Tokiwa, and T. Watanabe, T_c vs n relationship for multilayered high-T_c superconductors, J. Phys. Soc. Jpn. **76**, 094711 (2007).

[54] A. Schilling, M. Cantoni, J. D. Guo, and H. R. Ott, Superconductivity above 130 K in the Hg-Ba-Ca-Cu-O system, Nature (London) **363**, 56 (1993).

[55] L. Wang, X. Luo, J. Li, J. Zeng, M. Cheng, J. Freyermuth, Y. Tang, B. Yu, G. Yu, M. Greven, and Y. Li, Growth and characterization of $HgBa_2CaCu_2O_{6+\delta}$ and $HgBa_2Ca_2Cu_3O_{8+\delta}$ crystals, Phys. Rev. Mater. **2**, 123401 (2018).

[56] G. R. Stewart, Superconductivity in iron compounds, Rev. Mod. Phys. **83**, 1589 (2011).

[57] H. Hosono, A. Yamamoto, H. Hiramatsu, and Y. Ma, Recent advances in iron-based superconductors toward applications, Mater. Today **21**, 278 (2018).

[58] Z. Ren, W. Lu, J. Yang, W. Yi, X. Shen, G. Che, X. Dong, L. Sun, F. Zhou, and Z. Zhao, Superconductivity at 55 K in iron-based F-Doped Layered Quaternary Compound $Sm[O_{1-x}F_x]FeAs$, Chin. Phys. Lett. **25**, 2385 (2008).

[59] A. Iyo, K. Kawashima, T. Kinjo, T. Nishio, S. Ishida, H. Fujihisa, Y. Gotoh, K. Kihou, H. Eisaki, and Y. Yoshida, New-structure-type Fe-based superconductors: $CaAFe_4As_4$ (A = K, Rb, Cs) and $SrAFe_4As_4$ (A = Rb, Cs), J. Am. Chem. Soc. **138**, 3410 (2016).

[60] Z.-C. Wang, C.-Y. He, S.-Q. Wu, Z.-T. Tang, Y. Liu, A. Ablimit, C.-M. Feng, and G.-H. Cao, Superconductivity in $KCa_2Fe_4As_4F_2$ with separate double Fe_2As_2 layers, J. Am. Chem. Soc. **138**, 7856 (2016).

[61] T. Wang, C. Zhang, L. C. Xu, J. H. Wang, S. Jiang, Z. W. Zhu, Z. S. Wang, J. N. Chu, J. X. Feng, L. L. Wang, W. Li, T. Hu, X. S. Liu, and G. Mu, Strong Pauli paramagnetic effect in the upper critical field of $KCa_2Fe_4As_4F_2$, Sci. China Phys. Mech. Astron. **63**, 227412 (2020).

[62] H. Q. Yuan, J. Singleton, F. F. Balakirev, S. A. Baily, G. F. Chen, J. L. Luo, and N. L. Wang, Nearly isotropic superconductivity in (Ba, K)Fe_2As_2, Nature (London) **457**, 565 (2009).

[63] P. Richard, T. Sato, K. Nakayama, T. Takahashi, and H. Ding, Fe-based superconductors: An angle-resolved photoemission spectroscopy perspective, Rep. Prog. Phys. **74**, 124512 (2011).

[64] M. M. Parish, J. P. Hu, and B. A. Bernevig, Experimental consequences of the $s-$wave $\cos(k_x)\cos(k_y)$ superconductivity in the iron pnictides, Phys. Rev. B **78**, 144514 (2008).

[65] K. Seo, B. A. Bernevig, and J. Hu, Pairing Symmetry in a Two-Orbital Exchange Coupling model of Oxypnictides, Phys. Rev. Lett. **101**, 206404 (2008).

[66] P. J. Hirschfeld, M. M. Korshunov, and I. I. Mazin, Gap symmetry and structure of Fe-based superconductors, Rep. Prog. Phys. **74**, 124508 (2011).

[67] F. Wang and D. H. Lee, Science **332**, 200 (2011).

[68] I. Mazin and J. Schmalian, Pairing symmetry and pairing state in ferropnictides: Theoretical overview, Phyisca C: Supercond. **469**, 614 (2009).

[69] Y. Zhang, L. X. Yang, F. Chen, B. Zhou, X. F. Wang, X. H. Chen, M. Arita, K. Shimada, H. Namatame, M. Taniguchi, J. P. Hu, B. P. Xie, and D. L. Feng, Out-of-Plane Momentum and Symmetry-Dependent Energy Gap of the pnictide $Ba_{0.6}K_{0.4}Fe_2As_2$ Superconductor Revealed by Angle-Resolved Photoemission Spectroscopy, Phys. Rev. Lett. **105**, 117003 (2010).

[70] Y. Zhang, Z. R. Ye, Q. Q. Ge, F. Chen, J. Jiang, M. Xu, B. P. Xie, and D. L. Feng, Nodal superconducting-gap structure in ferropnictide superconductor $BaFe_2(As_{0.7}P_{0.3})_2$, Nat. Phys. **8**, 371 (2012).

[71] P. Materne, S. Kamusella, R. Sarkar, T. Goltz, J. Spehling, H. Maeter, L. Harnagea, S. Wurmehl, B. Bühner, H. Luetkens, C. Timm, and H.-H. Klauss, Coexistence of superconductivity and magnetism in $Ca_{1-x}Na_xFe_2As_2$: Universal suppression of the magnetic order parameter in 122 iron pnictides, Phys. Rev. B **92**, 134511 (2015).

[72] G. Wu, H. Chen, T. Wu, Y. L. Xie, Y. J. Yan, R. H. Liu, X. F. Wang, J. J. Ying, and X. H. Chen, Different resistivity response to spin-density wave and superconductivity at 20 K in $Ca_{1-x}Na_xFe_2As_2$, J. Phys.: Condens. Matter **20**, 422201 (2008).

[73] N. Haberkorn, B. Maiorov, M. Jaime, I. Usov, M. Miura, G. F. Chen, W. Yu, and L. Civale, Effect of doping on structural and superconducting properties in $Ca_{1-x}Na_xFe_2As_2$ single crystals ($x = 0.5$, 0.6, 0.75), Phys. Rev. B **84**, 064533 (2011).

[74] H. Zhou, Y. Zhang, Y. Li, S. Li, W. Hong, and H. Luo, Growth and characterization of superconducting $Ca_{1-x}Na_xFe_2As_2$ single crystals by NaAs-flux method, Chin. Phys. B **31**, 117401 (2022).

[75] U. Stuhr, B. Roessli, S. Gvasaliya, H. M. Rønnow, U. Filges, D. Graf, A. Bollhalder, D. Hohl, R. Bürge, M. Schild, L. Holitzner, C. Kaegi, P. Keller, and T. Mühlebach, The thermal triple-axis-spectrometer EIGER at the continuous spallation source SINQ, Nucl. Instrum. Methods Phys. Res., Sect. A **853**, 16 (2017).

[76] P. Giannozzi, O. Andreussi, T. Brumme, O. Bunau, M. Buongiorno Nardelli, M. Calandra, R. Car, C. Cavazzoni, D. Ceresoli, M. Cococcioni *et al.*, Advanced capabilities for materials modelling with Quantum ESPRESSO, J. Phys.: Condens. Matter **29**, 465901 (2017).

[77] L. Bellaiche, D. Vanderbilt, Virtual crystal approximation revisited: Application to dielectric and piezoelectric properties of perovskites, Phys. Rev. B **61**, 7877 (2000).

[78] D. V. Evtushinsky, V. B. Zabolotnyy, L. Harnagea, A. N. Yaresko, S. Thirupathaiah, A. A. Kordyuk, J. Maletz, S. Aswartham, S. Wurmehl, E. Rienks, R. Follath, B. Büchner, and S. V. Borisenko, Electronic band structure and momentum dependence of the superconducting gap in $Ca_{1-x}Na_xFe_2As_2$ from angle-resolved photoemission spectroscopy, Phys. Rev. B **87**, 094501 (2013).

[79] Y. Shi, Y. Huang, X. Wang, X. Shi, A. van Roekeghem, W. Zhang, N. Xu, P. Richard, T. Qian, E. Rienks, S. Thirupathaiah, K. Zhao, C. Jin, M. Shie, and H. Ding,

Observation of strong-coupling pairing with weakened Fermi-surface nesting at optimal hole doping in $Ca_{0.33}Na_{0.67}Fe_2As_2$, Chin. Phys. Lett. **31**, 067403 (2014).

[80] J. Zhao, D. T. Adroja, D. X. Yao, R. Bewley, S. Li, X. F. Wang, G. Wu, X. H. Chen, and P. C. Dai, Spin waves and magnetic exchange interactions in $CaFe_2As_2$, Nat. Phys. **5**, 555 (2009).

[81] M. Liu, L. W. Harriger, H. Luo, M. Wang, R. A. Ewings, T. Guidi, H. Park, K. Haule, G. Kotliar, S. M. Hayden, and P. Dai, Nature of magnetic excitations in superconducting $BaFe_{1.9}Ni_{0.1}As_2$, Nat. Phys. **8**, 376 (2012).

[82] M. Wang, C. Zhang, X. Lu, G. Tan, H. Luo, Y. Song, M. Wang, X. Zhang, E. A. Goremychkin, T. G. Perring, T. A. Maier, Z. Yin, K. Haule, G. Kotliar, and P. Dai, Doping dependence of spin excitations and its correlations with high-temperature superconductivity in iron pnictides, Nat. Commun. **4**, 2874 (2013).

[83] S. Ideta, N. Murai, M. Nakajima, R. Kajimoto, and K. Tanaka, Experimental investigation of the suppressed superconducting gap and double-resonance mode in $Ba_{1-x}K_xFe_2As_2$, Phys. Rev. B **100**, 235135 (2019).

[84] Y. Cai, J. Huang, T. Miao, D. Wu, Q. Gao, C. Li, Y. Xu, J. Jia, Q. Wang, Y. Huang, G. Liu, F. Zhang, S. Zhang, F. Yang, Z. Wang, Q. Peng, Z. Xu, L. Zhao, X. Zhou, Genuine electronic structure and superconducting gap structure in $(Ba_{0.6}K_{0.4})Fe_2As_2$ superconductor, Sci. Bull. **66**, 1839 (2021).

[85] D. Wu, W. Hong, C. Dong, X. Wu, Q. Sui, J. Huang, Q. Gao, C. Li, C. Song, H. Luo *et al.*, Spectroscopic evidence of bilayer splitting and strong interlayer pairing in the superconductor $KCa_2Fe_4As_4F_2$, Phys. Rev. B **101**, 224508 (2020).

[86] Y. Su, C. Setty, Z. Wang, and J. P. Hu, *c*-axis nodal lines induced by interlayer pairing in iron-based superconductors, Phys. Rev. B **85**, 184517 (2012).

[87] C. Liu, P. Bourges, Y. Sidis, T. Xie, G. He, F. Bourdarot, S. Danilkin, H. Ghosh, S. Ghosh, X. Ma, S. Li, Y. Li, and H. Luo, Preferred Spin Excitations in the Bilayer Iron-Based Superconductor $CaK(Fe_{0.96}Ni_{0.04})_4As_4$ with Spin-Vortex Crystal order, Phys. Rev. Lett. **128**, 137003 (2022).

[88] J. Guo, L. Yue, K. Iida, K. Kamazawa, L. Chen, T. Han, Y. Zhang, and Y. Li, Preferred Magnetic Excitations in the Iron-Based $Sr_{1-x}Na_xFe_2As_2$ Superconductor, Phys. Rev. Lett. **122**, 017001 (2019).

[89] T. Xie, C. Liu, F. Bourdarot, L.-P. Regnault, S. Li, and H. Luo, Spin-excitation anisotropy in the bilayer iron-based superconductor $CaKFe_4As_4$, Phys. Rev. Res. **2**, 022018(R) (2020).

[90] Y. Song, H. Man, R. Zhang, X. Lu, C. Zhang, M. Wang, G. Tan, L.-P. Regnault, Y. Su, J. Kang, R. M. Fernandes, and P. Dai, Spin anisotropy due to spin-orbit coupling in optimally hole-doped $Ba_{0.67}K_{0.33}Fe_2As_2$, Phys. Rev. B **94**, 214516 (2016).

[91] D. Hu, W. Zhang, Y. Wei, B. Roessli, M. Skoulatos, L.-P. Regnault, G. Chen, Y. Song, H. Luo, S. Li, and P. Dai, Spin excitation anisotropy in the optimally isovalent-doped superconductor $BaFe_2(As_{0.7}P_{0.3})_2$, Phys. Rev. B **96**, 180503(R) (2017).

[92] Z. R. Ye, Y. Zhang, F. Chen, M. Xu, J. Jiang, X. H. Niu, C. H. P. Wen, L. Y. Xing, X. C. Wang, C. Q. Jin, B. P. Xie, and D. L. Feng, Extraordinary Doping Effects on Quasiparticle Scattering and Bandwidth in Iron-Based Superconductors, Phys. Rev. X **4**, 031041 (2014).

[93] L. Wang, F. Hardy, A. E. Böhmer, T. Wolf, P. Schweiss, and C. Meingast, Complex phase diagram of $Ba_{1-x}Na_xFe_2As_2$: A multitude of phases striving for the electronic entropy, Phys. Rev. B **93**, 014514 (2016).

[94] K. M. Taddei, J. M. Allred, D. E. Bugaris, S. H. Lapidus, M. J. Krogstad, H. Claus, D. Y. Chung, M. G. Kanatzidis, R. Osborn, S. Rosenkranz, and O. Chmaissem, Observation of the magnetic C_4 phase in $Ca_{1-x}Na_xFe_2As_2$ and its universality in the hole-doped 122 superconductors, Phys. Rev. B **95**, 064508 (2017).

[95] K. M. Taddei, J. M. Allred, D. E. Bugaris, S. Lapidus, M. J. Krogstad, R. Stadel, H. Claus, D. Y. Chung, M. G. Kanatzidis, S. Rosenkranz, R. Osborn, and O. Chmaissem, Detailed magnetic and structural analysis mapping a robust magnetic $Sr_{1-x}Na_xFe_2As_2$, Phys. Rev. B **93**, 134510 (2016).

[96] J. M. Allred, K. M. Taddei, D. E. Bugaris, M. J. Krogstad, S. H. Lapidus, D. Y. Chung, H. Claus, M. G. Kanatzidis, D. E. Brown, J. Kang, R. M. Fernandes, I. Eremin, S. Rosenkranz, O. Chmaissem, and R. Osborn, Double-Q spin-density wave in iron arsenide superconductors, Nat. Phys. **12**, 493 (2016).

[97] S. Wu, Y. Song, Y. He, A. Frano, M. Yi, X. Chen, H. Uchiyama, A. Alatas, A. H. Said, L. Wang, T. Wolf, C. Meingast, and R. J. Birgeneau, Short-Range Nematic Fluctuations in $Sr_{1-x}Na_xFe_2As_2$ Superconductors, Phys. Rev. Lett. **126**, 107001 (2021).

[98] K. Zhao, Q. Q. Liu, X. C. Wang, Z. Deng, Y. X. lv, J. L. Zhu, F. Y. Li, and C. Q. Jin, Superconductivity above 33 K in $(Ca_{1-x}Na_x)Fe_2As_2$, J. Phys. Condens. Matter **22**, 222203 (2010).

[99] Y. Mizuguchi, Y. Hara, K. Deguchi, S. Tsuda, T. Yamaguchi, K. Takeda, H. Kotegawa, H. Tou, and Y. Takano, Anion height dependence of T_c for the Fe-based superconductor, Supercond. Sci. Technol. **23**, 054013 (2010).

[100] C. H. Lee, K. Kihou, A. Iyo, H. Kito, P. M. Shirage, and H. Eisaki, Relationship between crystal structure and superconductivity in iron-based superconductors, Solid State Commun. **152**, 644 (2012).